Cloaking of a vertical cylinder in waves using variable bathymetry

R. Porter[1,†] and J. N. Newman[2]

[1]School of Mathematics, University of Bristol, Bristol, BS8 1TW, UK

[2]Department of Mechanical Engineering, MIT, Cambridge, MA 02139, USA

The paper describes a process which allows a vertical circular cylinder subject to plane monochromatic surface gravity waves to appear invisible to the far-field observer. This is achieved by surrounding the cylinder with an annular region of variable bathymetry. Two approaches are taken to investigate this effect. First a mild-slope approximation is applied to the governing linearised three-dimensional water wave equations to formulate a depth-averaged two-dimensional wave equation with varying wavenumber over the variable bathymetry. This is then solved by formulating a domain integral equation, solved numerically by discretisation. For a given set of geometrical and wave parameters, the bathymetry is selected by a numerical optimisation process and it is shown that the scattering cross-section is reduced towards zero with increasing refinement of the bathymetry. A fully three-dimensional boundary-element method, based on the WAMIT solver (see www.wamit.com) but adapted here to allow for depressions in the bed, is used to assess the accuracy of the mild-slope results and then further numerically optimise the bathymetry towards a cloaking structure. Numerical results provide strong evidence that perfect cloaking is possible for the fully three-dimensional problem. One practical application of the results is that cloaking implies a reduced mean drift force on the cylinder.

Key words: surface gravity waves, wave scattering, wave-structure interactions

---

1. Introduction

The idea of rendering objects placed in a wavefield to appear invisible to the far-field observer has been given the name 'cloaking'. Attempts at cloaking using absorbing and anti-reflection devices extend back over many decades, mainly applied to the area of electromagnetic theory. Interest in this subject was re-ignited by the simultaneous publications of Leonhardt (2006) and Pendry, Schurig & Smith (2006), both of whom showed the principle of a perfect cloaking mechanism.

Pendry *et al.* (2006) use the invariance of Maxwell's equations for electromagnetism under a change of coordinate system, provided that the material parameters (permittivity and permeability) are suitably rescaled (Ward & Pendry 1996). Leonhardt (2006) applied essentially the same principle in a two-dimensional geometric optics

† Email address for correspondence: richard.porter@bris.ac.uk

setting through the use of conformal mappings. The invariance property of the governing equations allows mappings to be constructed from a problem in which waves propagate uninterrupted through free space into a problem with a circular (in two dimensions) or spherical (in three dimensions) inclusion surrounded by an annular region with varying material parameters. Waves entering the cloak are now bent around the obstacle rendering it invisible to the observer in the far field.

The concept of cloaking has been applied to other physical wave systems, most notably to waves in an acoustic medium where a similar mapping technique can be formulated in both two and three dimensions: see Chen & Chan (2007), Cummer *et al.* (2007) and Cummer & Schurig (2007). Now the density and bulk modulus of a cloaking material surrounding the inclusion must be designed to vary in a particular manner, determined by the mapping, to deflect waves around the device. In three-dimensional elasticity, Milton, Briane & Willis (2006) showed that Navier's elasticity equations are not invariant under a coordinate transformation although Farhat *et al.* (2009) have shown that in thin two-dimensional elastic Euler–Bernoulli plates a mapping technique can be used to effect a cloaking device.

There is more limited work in the area of cloaking for surface waves on a fluid, perhaps because the scope for physical application is limited. Farhat *et al.* (2008) studied surface waves in the gravity–capillary length scale, using a cloak comprised of an annular domain containing a large periodic array of small vertical circular posts. Here, the incident wavelength is large compared to the dimension of the posts in the cloaking device, though small compared to the inclusion being cloaked. Established homogenisation techniques are used to capture the effect of the posts in a continuum model which includes the components of anisotropy required of a model cloak derived under the transformation technique. Farhat *et al.* (2008) were then able to design the structure of the array of posts to achieve the correct radial behaviour of their anisotropic shear modulus tensor although admitted that an extra degree of flexibility needed for the design of a perfect cloak, that of radially varying density, was not possible under the homogenisation model. Nevertheless, experiments are presented alongside the theory showing the cloak to be effective. Another paper, Alam (2012), shows how cloaking of an object floating in the surface can be achieved in a two-dimensional setting in the presence of a two-layer stratified fluid, using a series of sinuisoidal bottom corrugations to transfer energy from incoming surface waves into interfacial waves which pass below the surface object before being transformed back into surface waves by another series of bottom corrugations on the other side of the object.

In this paper we consider the cloaking of a cylinder by surface waves on a fluid. Specifically, we consider using changes in the fluid depth as a mechanism for cloaking a vertical circular cylinder. Thus, it is well known that surface waves are refracted by changes in depth (see Mei 1983 for example). These effects are often studied using either a long-wave/shallow-water model or a geometric optics approach (ray theory) for high-frequency waves. Both approaches remove explicit depth dependence from the underlying equations of surface waves to leave two-dimensional equations in the surface. Attempts at using these reduced equations to suggest ways in which either long waves, or short waves, might be bent around a cylinder have proved unsuccessful.

Further efforts to apply the coordinate transformation method described previously to the linearised water wave problem also seem unlikely to succeed. There are two issues. First, although it is possible to envisage a physical problem in which the depth is anisotropic (for example, the depth profile of the bed could be comprised of interleaving narrow vertical combs whose profiles in the radial and azimuthal

directions may be different) the fact remains that the transformation method (whose map is not area preserving) requires two 'material' parameters to be varying in the domain and here we may only control the depth. Second, whilst the governing field equation (Laplace's equation) can be preserved under a conformal mapping of the horizontal coordinates, the required rescaling of the vertical coordinate implies that the boundary conditions on the free surface and the bottom bed are not preserved. This obstacle seems particular to the water wave problem, since lateral boundary conditions do not exist in the other problems cited previously for other types of wavefields.

Given the preceding arguments it seems unlikely that a cloak can be designed for surface waves in a homogeneous fluid by varying the fluid depth. Thus we have moved back from what is now usually defined as cloaking in which a 'dead zone', devoid of fluid motion and waves, is created and within which an object of arbitrary shape can be hidden from the far-field observer. Instead, we focus on the question of whether it is possible to cloak an object of a specific shape having a specific boundary condition upon its surface. This is analogous to the idea used by Alù & Engheta (2005), whose work preceded Leonhardt (2006) and Pendry *et al.* (2006), who considered cloaking of transverse magnetic/electric (TM or TE) polarised electromagnetic waves by surrounding a single dielectric layer with given permittivity and permeability with an annular region of a different (but constant) permittivity and permeability. Alù & Engheta (2005) showed that, for large wavelength-to-cylinder ratios, low visibility could be obtained at certain frequencies. They appealed to the idea that, in this limit, the uncloaked cylinder scattering pattern is predominantly dipolar and that a destructive interference effect could be introduced by adding an annular cloaking domain with appropriately chosen dielectric constants. This idea lends itself well to surface gravity waves which are typically thought of as long compared to the size of a typical scattering object. We use a vertical circular cylinder extending throughout the depth as the scattering object, mainly because of its simplicity, although we are not suggesting that this is the only object that we could have chosen. Surrounding the cylinder is an annular region of varying bathymetry which is described by a finite expansion of orthogonal functions in the radial and azimuthal directions. By allowing more than one degree of freedom in the bed, we do not restrict ourselves to the low-frequency limit used by Alù & Engheta (2005). By adjusting the weighting of each component of the bathymetry via a numerical optimisation process, we aim to lower the scattering cross-section from the uncloaked cylinder, with a limit of zero representing the perfect cloak.

The outline of the rest of the paper is as follows. In §2, we give a statement of the problem of a cylinder surrounded by varying bathymetry. In §3 an approximation based on the mild-slope equation (MSE) is described, in which the complexity of the fully three-dimensional boundary-value problem is reduced by depth-averaging to a simpler two-dimensional wave equation with a spatially varying wavenumber. A domain integral equation is derived, adapting recent work by Griffiths & Porter (2012) to account for the cylinder. Section 4 describes a fully three-dimensional boundary-element method which is based on an adaptation of the WAMIT solver (www.wamit.com) to account for depressions in the bed below the depth at infinity. In §5 the optimisation procedure used to achieve cloaking is described, and results are presented for axisymmetric and non-axisymmetric beds.

The inclusion of the approximate MSE model in the paper serves a variety of purposes. First, it accurately reflects the progression of work that was undertaken on this problem, being originally instigated by Porter (2011) using MSE before being

pursued by Newman (2012) using a full linear theory (FLT) to validate and refine the MSE results. Second, the use of FLT in conjunction with an approximation which, from a numerical standpoint is completely unrelated, is useful for gathering evidence to support the existence of cloaking. This is particularly pertinent given that results from WAMIT are only single precision and, taken by themselves, are not conclusive. Thus evidence that a different model (albeit approximate) using double-precision code is able to predict cloaking to a higher degree of accuracy is important.

2. Formulation of the problem

We adopt cylindrical polar coordinates $(r, \theta, z) \equiv (\mathbf{r}, z)$ with $z = 0$ coinciding with the mean free surface of the fluid and z pointing vertically upwards. An impermeable vertical cylinder with constant circular cross-section of radius a is centred along the z-axis and extends throughout the depth. The sea-bed is defined by $z = -h(\mathbf{r})$ for $r > a$. Here $h(\mathbf{r})$ is a continuous function with continuous derivatives, and $h(\mathbf{r}) = h_0$, a constant, for $r > b$. Thus, the bed is allowed to vary in the annular region $a < r < b$.

We adopt linearised water wave theory in which the velocity potential is given by $\mathrm{Re}\{\Phi(\mathbf{r}, z)\exp(-\mathrm{i}\omega t)\}$ where ω is the assumed angular frequency of motion. Then Φ satisfies

$$(\nabla^2 + \partial_{zz})\Phi = 0, \quad -h(\mathbf{r}) < z < 0, \ r > a, \ 0 \leqslant \theta < 2\pi, \tag{2.1}$$

where $\mathbf{\nabla} = (\partial_r, r^{-1}\partial_\theta)$,

$$\Phi_z - K\Phi = 0 \quad \text{on } z = 0, \ r > a, \tag{2.2}$$

where $K = \omega^2/g$, g is gravitational acceleration, and

$$\Phi_z + \nabla h \cdot \nabla \Phi = 0 \quad \text{on } S_b := \{z = x - h(\mathbf{r}), \ r > a\}, \tag{2.3}$$

which reduces to $\Phi_z = 0$ on $z = -h_0$ for $r > b$. On the cylinder, $\mathbf{r} = \mathbf{r}_a = (a, \theta)$ we have

$$\Phi_r(\mathbf{r}_a, z) = 0 \quad \text{on } S_c := \{-h(\mathbf{r}_a) < z < 0, \ 0 \leqslant \theta < 2\pi\}. \tag{2.4}$$

An incident wave propagating in the direction β is given by the potential

$$\Phi_{inc}(\mathbf{r}, z) = \exp(\mathrm{i}k_0 r \cos(\theta - \beta)) \, w(k_0 h_0, k_0 z), \tag{2.5}$$

where

$$w(p, q) = \frac{\cosh(p + q)}{\cosh p}, \tag{2.6}$$

and $k = k_0$ is the real positive root corresponding to $h = h_0$ of

$$k \tanh kh = K. \tag{2.7}$$

The total potential is $\Phi = \Phi_{inc} + \Phi_{sc}$ where Φ_{sc} is a potential representing the scattered waves which therefore satisfies the radiation condition and hence

$$\Phi_{sc}(\mathbf{r}, z) \sim \mathscr{A}(\theta; \beta)\sqrt{\frac{2}{\pi k_0 r}} \exp(\mathrm{i}(k_0 r - \pi/4)) \, w(k_0 h_0, k_0 z) \quad \text{as } k_0 r \to \infty, \tag{2.8}$$

where $\mathscr{A}(\theta; \beta)$ measures the circular scattered wave amplitude in the direction θ due to a wave incident in the direction β. The dependence of various quantities on β is made explicit where later reference is required.

In order that the cylinder be cloaked it is required that $\mathscr{A}(\theta; \beta) \equiv 0$ for $0 \leqslant \theta < 2\pi$. Alternatively, the total energy scattered to infinity (the scattering cross-section)

$$\mathscr{E} = \frac{1}{2\pi} \int_0^{2\pi} |\mathscr{A}(\theta; \beta)|^2 \mathrm{d}\theta = -\mathrm{Re}\{\mathscr{A}(\beta; \beta)\} \tag{2.9}$$

must be zero. The final equality in (2.9) is a well-known result originally derived by Maruo (1960) in the water wave context. In other contexts it is known as the optical theorem.

If $h(\mathbf{r}) = h_0$ for all $r > a$ so the bed is flat everywhere, then the exact solution is well known (e.g. Mei 1983) and given by

$$\Phi_{cyl}(\mathbf{r}, z) = \psi_{cyl}(\mathbf{r}; \beta)w(k_0 h_0, k_0 z), \tag{2.10}$$

where

$$\psi_{cyl}(\mathbf{r}; \beta) = \sum_{n=-\infty}^{\infty} \mathrm{i}^n \left(\mathrm{J}_n(k_0 r) - Z_n \mathrm{H}_n(k_0 r)\right) \exp\left(\mathrm{i}n(\theta - \beta)\right). \tag{2.11}$$

Here J_n and $\mathrm{H}_n \equiv \mathrm{H}_n^{(1)}$ are Bessel and Hankel functions, and $Z_n = \mathrm{J}_n'(k_0 a)/\mathrm{H}_n'(k_0 a)$. Thus the scattering amplitude for the flat bed is given by

$$\mathscr{A}_{cyl}(\theta; \beta) = -\sum_{n=-\infty}^{\infty} Z_n \exp\left(\mathrm{i}n(\theta - \beta)\right). \tag{2.12}$$

The total scattered wave energy (2.9) equates to

$$\mathscr{E}_{cyl} = \sum_{n=-\infty}^{\infty} |Z_n|^2 = \mathrm{Re}\left\{\sum_{n=-\infty}^{\infty} Z_n\right\}, \tag{2.13}$$

which is independent of β as expected, and never zero.

3. The mild-slope approximation

In this section the problem formulated in §2 is approximated by employing the mild-slope method. That is, the potential locally assumes the depth-dependence assigned to propagating modes over a locally flat bed of the same depth,

$$\Phi(\mathbf{r}, z) \approx \phi(\mathbf{r})w(kh, kz), \tag{3.1}$$

in which $k(\mathbf{r}) = k(h)$ denotes the positive, real root of (2.7) and the depth, $h(\mathbf{r})$, is now varying spatially. We follow the implementation of the approximation (3.1) of Chamberlain & Porter (1995) which uses a variational principle to replace (2.1)–(2.3) by the single modified mild-slope equation (MMSE), namely

$$\nabla \cdot (u_0 \nabla \phi) + \left(k_0^2 u_0 + u_1 \nabla^2 h + u_2 (\nabla h)^2\right) \phi = 0, \quad r > a, \tag{3.2}$$

where $u_0(h) = \mathrm{sech}^2 kh(2kh + \sinh 2kh)/(4k)$ and $u_1(h)$, $u_2(h)$ are given by Chamberlain & Porter (1995) but are not required explicitly here. In addition, the boundary condition (2.4) on the cylinder gives rise, from the variational principle, to the natural condition requiring

$$\int_{-h}^{0} w \left.\frac{\partial(w\phi)}{\partial r}\right|_{r=a} \mathrm{d}z = 0, \quad 0 \leqslant \theta < 2\pi. \tag{3.3}$$

After integrating, this gives the (rather unintuitive) boundary condition on the reduced potential ϕ to be

$$u_0\phi_r + u_1 h_r\phi = 0 \quad \text{on } r = a. \tag{3.4}$$

This condition is overlooked in later work of Chamberlain & Porter (1999) and also in Porter (2011), but is taken into account in a recent paper of Liu, Wang & Tang (2013).

A transformation of (3.2) into its canonical form is achieved by writing

$$\phi(\boldsymbol{r}) = \{u_0(h_0)/u_0(h(\boldsymbol{r}))\}^{1/2}\,\psi(\boldsymbol{r}), \tag{3.5}$$

upon which ψ can be shown to satisfy (e.g. Griffiths & Porter 2012)

$$\nabla^2\psi + \kappa(\boldsymbol{r})\psi = 0, \quad r > a, \tag{3.6}$$

where

$$\kappa(\boldsymbol{r}) = k_0^2 + A(h)\nabla^2 h + B(h)(\nabla h)^2, \tag{3.7}$$

and $A(h)$, $B(h)$ are now functions of u_0, u_1 and u_2 whose definitions can be found in Griffiths & Porter (2012). Application of (3.5) to (3.4) leads to the boundary condition

$$\psi_r + h_r A(h)\psi = 0 \quad \text{on } r = a,\ 0 \leqslant \theta < 2\pi. \tag{3.8}$$

Finally we mimic the decomposition of Φ by writing $\psi(\boldsymbol{r}) = \psi_{inc}(\boldsymbol{r}) + \psi_{sc}(\boldsymbol{r})$ where $\psi_{inc}(\boldsymbol{r}) = \exp\,(\mathrm{i}k_0 r\cos(\theta - \beta))$, and

$$\psi_{sc}(\boldsymbol{r}) \sim \mathscr{A}(\theta; \beta)\sqrt{\frac{2}{\pi k_0 r}}\exp(\mathrm{i}(k_0 r - \pi/4)). \tag{3.9}$$

We briefly remark that the reduced potential ψ_{cyl} defined in (2.11) and used to express the solution of the exact scattering by a circular cylinder on a flat bed is also (and unsurprisingly) an exact solution of the MMSE with $\mathscr{A}(\theta; \beta)$ replaced by $\mathscr{A}_{cyl}(\theta; \beta)$ as defined in (2.12).

We now follow closely the method described in Griffiths & Porter (2012), reformulating the wave equation (3.6) into an integral equation using a Green function $G(\boldsymbol{r}; \boldsymbol{r}')$ satisfying

$$(\nabla^2 + k_0^2)G = \delta(\boldsymbol{r} - \boldsymbol{r}'), \tag{3.10}$$

with $\boldsymbol{r}'$ representing the field point (r', θ') and $G_r(\boldsymbol{r}_a; \boldsymbol{r}') = 0$. It can readily be shown that

$$G(\boldsymbol{r}; \boldsymbol{r}') = -\frac{\mathrm{i}}{4}\mathrm{H}_0(k_0\rho) + \frac{\mathrm{i}}{4}\sum_{n=-\infty}^{\infty} Z_n\mathrm{H}_n(k_0 r)\mathrm{H}_n(k_0 r')\exp\left(\mathrm{i}n(\theta - \theta')\right), \tag{3.11}$$

where $\rho^2 = |\boldsymbol{r} - \boldsymbol{r}'|^2 \equiv r^2 + r'^2 - 2rr'\cos(\theta - \theta')$ and with Z_n defined following (2.11). The result of applying Green's identity to $\psi - \psi_{cyl}$ and G over the infinite domain $r > a$, $0 \leqslant \theta < 2\pi$ is

$$\psi(\boldsymbol{r}') + \iint_D \left[\kappa(\boldsymbol{r}) - k_0^2\right] G(\boldsymbol{r}; \boldsymbol{r}')\psi(\boldsymbol{r})\, r\mathrm{d}r\mathrm{d}\theta$$
$$- \int_0^{2\pi} A(h(\boldsymbol{r}_a))h_r(\boldsymbol{r}_a)G(\boldsymbol{r}_a; \boldsymbol{r}')\psi(\boldsymbol{r}_a)\, a\mathrm{d}\theta = \psi_{cyl}(\boldsymbol{r}'; \beta) \tag{3.12}$$

for $|\boldsymbol{r}'| \geqslant a$, where ψ_{cyl} is defined by (2.11) and $D := \{a < r < b,\ 0 < \theta < 2\pi\}$ is the projection of the varying bed S_b onto the (r, θ)-plane. The boundary integral on $\partial D := \{r = a,\ 0 \leqslant \theta < 2\pi\}$ appears during the application of (3.8). Thus (3.12) serves

as an integral equation for the unknown ψ when $\boldsymbol{r}'$ is restricted to $D \cup \partial D$ and defines ψ beyond D once ψ is known in $D \cup \partial D$.

Taking $k_0 r' \to \infty$ allows us to access the far-field behaviour of ψ which, in comparison with (3.9), gives

$$
\mathscr{A}(\theta'; \beta) = \mathscr{A}_{cyl}(\theta'; \beta) + \frac{\mathrm{i}}{4} \iint_D \left[\kappa(\boldsymbol{r}) - k_0^2 \right] \psi_{cyl}(\boldsymbol{r}; \theta' + \pi) \psi(\boldsymbol{r}) \, r \mathrm{d}r \mathrm{d}\theta
$$
$$
- \frac{\mathrm{i}}{4} \int_0^{2\pi} A(h(\boldsymbol{r}_a)) h_r(\boldsymbol{r}_a) \psi_{cyl}(\boldsymbol{r}_a; \theta' + \pi) \psi(\boldsymbol{r}_a) \, a \mathrm{d}\theta, \tag{3.13}
$$

where $\mathscr{A}_{cyl}$ is defined by (2.12). In deriving the above, we have made use of the leading-order large-argument expansion of the Hankel function in (3.11).

The strategy is to determine solutions $\psi(\boldsymbol{r})$ over $\boldsymbol{r} \in D \cup \partial D$ from (3.12) and use these solutions to calculate $\mathscr{A}(\theta'; \beta)$ from (3.13). Finally, the scattering cross-section $\mathscr{E}$ can be found using (2.9).

Solutions to (3.12) are approximated numerically using a discretisation approach similar to that described by Griffiths & Porter (2012, §4.2), thereby allowing the scattering coefficients to be approximated from (3.13). The approximation method is unsophisticated and uses piecewise-constant values for the unknown ψ on an N by M polar grid over the annular domain $D \cup \partial D$. However, the approximation to the integral equations is based on Galerkin's method, and therefore converges rapidly with increasing values of N and M. An added consequence of using Galerkin's method is that (2.9) is satisfied automatically to machine precision for any values of M and N. However, the procedure is still numerically intensive, requiring the inversion of full $MN \times NM$ matrices. Symmetries in the bathymetry can be exploited to reduce the domain of the integral equation to a quarter of its original size and this improves the numerical efficiency.

When the bathymetry is axisymmetric the MSE problem can be reformulated by expanding the azimuthal variation of both unknown quantities and Green functions into Fourier modes. This leads to an infinite series of simpler one-dimensional integral equations for each azimuthal mode which involves non-singular Green functions. This is easier to code and significantly quicker computationally than the non-axisymmetric counterpart, exhibiting rapid convergence with increasing terms in the series, and has been used for all computations involving axisymmetric beds. It also allows the MSE results to be validated against the full system when axisymmetry has not been assumed. Results have also been validated against those produced by the method of Griffiths & Porter (2012) for the case of no cylinder, by letting the radius of the circular cylinder shrink towards zero. Further validation against fully three-dimensional calculations will follow in §5.

4. Fully three-dimensional calculations

In a fluid of constant depth the scattering characteristics of a body can be analysed using the panel method (see, for example, Lee & Newman 2004). A boundary-integral equation for the unknown velocity potential is derived, using the Green function which satisfies the boundary conditions on the free surface and bottom and the radiation condition in the far field. The domain of the integral equation is restricted to the submerged surface S of the body. After discretization the integral equation is reduced to a linear system of algebraic equations. This method can be extended to cases with variable bathymetry where $h(x, y) \leqslant h_0$, by extending S to include S_b, the bottom

in the region of varying depth. Ferreira & Newman (2009) used this approach to analyse wave effects on a ship above a sloping bottom. However it cannot be used if $h(x, y) > h_0$, as is the case for bathymetry suggested by results indicated by the MSE approach later in § 5, since the Green function which satisfies the boundary condition on $z = -h_0$ is singular if $z < -h_0$. This restriction could be avoided by using a different Green function, e.g. corresponding to the maximum depth or infinite depth, but the resulting computational domain would include the entire bottom extending to infinity. Instead we consider a more efficient approach based on domain decomposition, with a matching boundary between the interior domain with variable bathymetry and the exterior domain with constant depth. Matching boundaries have been used for a variety of wave–body problems, especially for cases involving thin vertical barriers and bodies with vertical sides. Belibassakis (2008) and Pinkster (2011) have used matching with panel methods to analyse problems with other types of bathymetry.

Two domains D_i ($i = 0, 1$) are considered, with the corresponding velocity potentials denoted by $\Phi^{(i)}$. The exterior domain D_0 extends to infinity, with constant depth h_0. In the interior domain D_1 the depth $h(x, y)$ is arbitrary, except that it must match the depth h_0 on the matching boundary, S_m. The boundary surface of D_1, not including the free surface, is $S_1 = S_c \cup S_b \cup S_m$ where S_c denotes the wetted surface of the vertical cylinder and S_b represents the varying bed within D_1. The potential $\Phi^{(0)}$ includes the incident wave Φ_{inc} defined by (2.5) and the scattering component Φ_{sc} which satisfies the radiation condition in the far field given by (2.8). The matching boundary S_m separates the two domains, extending from the bottom $z = -h_0$ to the free surface $z = 0$. The unit normal is defined to point out of the domain D_i on its boundary.

Green's second identity is applied separately in each domain. Thus for field points $\boldsymbol{x}$ on the boundary surface S_i,

$$2\pi \Phi^{(i)}(\boldsymbol{x}) + \iint_{S_i} \left(\Phi^{(i)}(\boldsymbol{\xi}) \frac{\partial G^{(i)}(\boldsymbol{\xi}; \boldsymbol{x})}{\partial n_{\boldsymbol{\xi}}} - G^{(i)}(\boldsymbol{\xi}; \boldsymbol{x}) \frac{\partial \Phi^{(i)}(\boldsymbol{\xi})}{\partial n_{\boldsymbol{\xi}}} \right) \mathrm{d}S_{\boldsymbol{\xi}}$$
$$= \begin{cases} 4\pi \Phi_{inc}(\boldsymbol{x}), & i = 0, \\ 0, & i = 1. \end{cases} \tag{4.1}$$

Here $G^{(1)}(\boldsymbol{\xi}; \boldsymbol{x})$ is any Green function which is regular within D_1 (except at the source point $\boldsymbol{\xi}$, where $G^{(1)} \sim 1/|\boldsymbol{\xi} - \boldsymbol{x}|$), and satisfies the free-surface condition. For simplicity the conventional free-surface Green function for infinite depth is used. $G^{(0)}$ is the Green function for finite depth, h_0. For the specification of both types of Green function see Mei (1983). The term $4\pi \Phi_{inc}$ is included on the right-hand side since $\Phi^{(0)}$ does not satisfy the radiation condition.

On S_b and S_c (2.3) and (2.4) hold and so the normal velocity $\Phi_n^{(1)} = 0$, where the subscript n denotes the normal derivative. The appropriate boundary conditions on S_m are $\Phi^{(0)} = \Phi^{(1)}$ and $\Phi_n^{(0)} = -\Phi_n^{(1)}$, expressing continuity of pressure and normal velocity respectively. Using (4.1), writing separate equations for the two domains and invoking the boundary conditions on S_m gives the following three equations:

$$2\pi \Phi^{(1)} + \iint_{S_b \cup S_c} \Phi^{(1)} G_n^{(1)} \mathrm{d}S_{\boldsymbol{\xi}} + \iint_{S_m} \Phi^{(0)} G_n^{(1)} \mathrm{d}S_{\boldsymbol{\xi}} + \iint_{S_m} G^{(1)} \Phi_n^{(0)} \mathrm{d}S_{\boldsymbol{\xi}} = 0, \quad (4.2)$$

$$2\pi \Phi^{(0)} + \iint_{S_b \cup S_c} \Phi^{(1)} G_n^{(1)} \mathrm{d}S_{\boldsymbol{\xi}} + \iint_{S_m} \Phi^{(0)} G_n^{(1)} \mathrm{d}S_{\boldsymbol{\xi}} + \iint_{S_m} G^{(1)} \Phi_n^{(0)} \mathrm{d}S_{\boldsymbol{\xi}} = 0, \quad (4.3)$$

$$2\pi \Phi^{(0)} + \iint_{S_m} \Phi^{(0)} G_n^{(0)} \mathrm{d}S_{\boldsymbol{\xi}} - \iint_{S_m} G^{(0)} \Phi_n^{(0)} \mathrm{d}S_{\boldsymbol{\xi}} = 4\pi \Phi_{inc}, \quad (4.4)$$

where (4.2) is applied on $x \in S_b \cup S_c$, and (4.3), (4.4) on $x \in S_m$. In the above equations, arguments have been dropped so that $G_n^{(i)}$ is shorthand for $\partial G^{(i)}(\xi; x)/\partial n_\xi$. The unknowns in (4.2)–(4.4) are $\Phi^{(1)}$ on $S_b \cup S_c$ and $\Phi^{(0)}$, $\Phi_n^{(0)}$ on S_m. The coupled integral equations (4.2)–(4.4) are discretised and solved using a modified version of the panel code WAMIT. The higher-order method is used, with the unknowns represented by B-splines as explained by Lee & Newman (2004). The surfaces S_b and S_c are represented by explicit formulae and S_m is defined to be a circular cylinder of radius b, as in the previous section.

Using $\Phi^{(0)}$ and the function $\exp(-ik_0 r \cos(\theta - \theta'))w(k_0 z, k_0 h_0)$ in Green's second identity applied to the domain D_0 which extends to infinity, the following relation for the far-field scattering amplitude can be found:

$$\mathscr{A}(\theta'; \beta) = -\frac{igk_0}{4\omega v_g} \iint_{S_m} \left(\Phi_n^{(0)} - \Phi^{(0)} \frac{\partial}{\partial n} \right) \frac{\cosh(k_0(z + h_0))}{\cosh(k_0 h_0)} \exp\left(-ik_0 r \cos(\theta - \theta')\right) \, dS,$$

(4.5)

where v_g is the group velocity in depth h_0. In terms of the Kochin function $H(\theta)$ (e.g. Wehausen & Laitone 1960) the relation $H(\theta) = 2i\mathscr{A}(\theta; \beta)$ holds.

Once $\mathscr{A}(\theta; \beta)$ has been computed from (4.5), the total scattered energy in waves radiated to infinity is computed from (2.9).

5. Numerical results

5.1. *The bathymetry and cloaking procedure*

We are interested in the 'cloaking factor'

$$\mathscr{C} = \frac{\mathscr{E}}{\mathscr{E}_{cyl}},$$

(5.1)

where $\mathscr{E}_{cyl}$ defined by (2.13) is the scattering cross-section for a flat bed and $\mathscr{E}$ is defined for the variable bathymetry by (2.9) with $\mathscr{A}$ defined by (3.13) under the MSE approximation and (4.5) for fully three-dimensional computations. When $\mathscr{C} < 1$, the cylinder with the cloaking region containing the variable bathymetry scatters less energy than with a flat bed. Perfect cloaking requires $\mathscr{C} = 0$.

In order to consider varying bed shapes of a general form, the depth $h(r, \theta)$ is defined by a Fourier–Chebychev basis with

$$h(r, \theta) = h_0 + \sum_{p=1}^{P} \sum_{q=1}^{Q} \alpha_{p,q} f_p(r) \cos(2(q - 1)\theta),$$

(5.2)

where

$$f_p(r) = \frac{1}{2} T_{2p} \left(\frac{b - r}{b - a} \right) - \frac{1}{2}(-1)^p,$$

(5.3)

and $T_n(\cdot)$ are orthogonal Chebychev polynomials. The particular choice in (5.3) ensures that $h(b, \theta) = h_0$ and $h_r(b, \theta) = 0$ as required by the MSE approach. The reasoning behind the choice of Chebychev polynomials is that more refinement in the bed was expected as the cylinder is approached. Our results support this hypothesis. The expansion in θ dictates that the bed shape is symmetric about both planes $\theta = 0$ and $\theta = \pi/2$. We have assumed that the objective is to cloak for an incident wave angle of $\beta = 0$ and this is most likely to be successful if symmetry is assumed in the bathymetry about the plane $\theta = 0$. Symmetry of the bathymetry in the plane $\theta = \pi/2$, perpendicular to the assumed wave direction, is motivated by the following argument. Suppose a bathymetry cloaks the cylinder for waves from one direction such that the incident wavefield is perfectly reconstructed downwave of the cylinder and there are
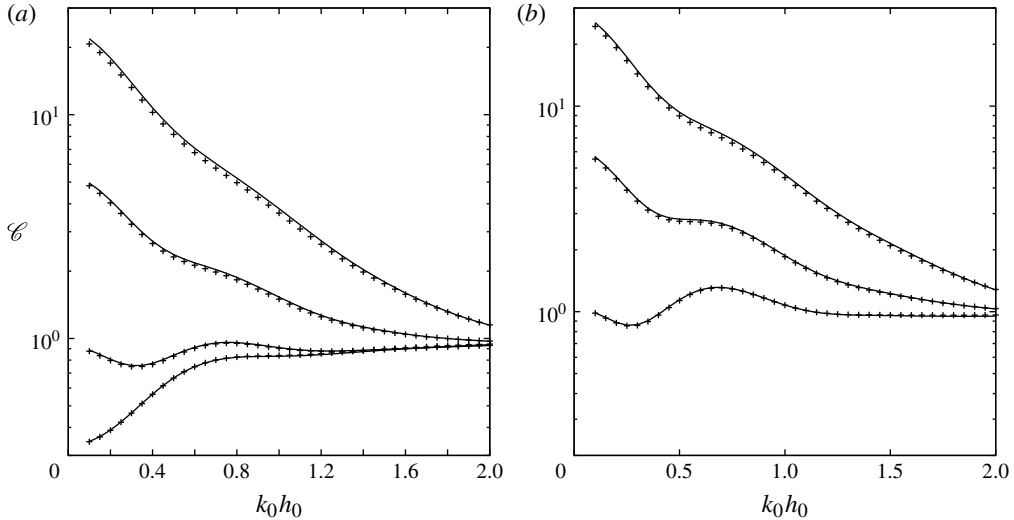
FIGURE 1. Comparison of $\mathscr{C}$ against k_0h_0 computed using MSE (solid lines) and FLT (crosses) for axisymmetric beds with one radial basis mode: (*a*) $\alpha_{1,1} = 0.1, 0.2, 0.4, 0.8$; (*b*) $\alpha_{1,1} = 0$, $\alpha_{2,1} = -0.1, -0.2, -0.4$. In both examples, $\mathscr{C}$ increases with increasing magnitude of the coefficients.

no outgoing circular diffracted waves. Assuming that this solution is described by Φ, consider now the problem described by the complex-conjugate potential $\overline{\Phi}$. This satisfies all of the conditions of the original problem apart from that the incident wave has reversed direction and hence the reflection of the original cloaking bathymetry about the plane $\theta = \pi/2$ must also be a cloaking bathymetry. If a cloaking bathymetry were unsymmetric about $\theta = \pi/2$, then a second independent cloaking bathymetry would be guaranteed by this argument. This seems unlikely although we do not rule this possibility out. It has also been confirmed numerically that the contribution from odd cosine modes plays a negligible role in reducing the value of $\mathscr{C}$.

Before considering attempts at cloaking, the results from the MSE and FLT are compared for simple bed shapes. In figure 1(*a*,*b*) the variation of $\mathscr{C}$ is shown against k_0h_0 for axisymmetric beds ($Q = 1$) with $a/h_0 = 1/2$, $b/h_0 = 5$. In figure 1(*a*) $P = 1$ has been chosen with $\alpha_{1,1} = 0.1, 0.2, 0.4, 0.8$. Figure 1(*b*) shows results for $P = 2$, $\alpha_{1,1} = 0$, $\alpha_{2,1} = -0.1, -0.2, -0.4$. A log scale on the vertical axis helps separate results in each figure. The computations from the MSE and FLT are in good agreement, with only small differences emerging for steeper beds and small values of k_0h_0. These observations are consistent with the range of validity of the MSE and other comparisons between the MSE and FLT (see, for example, Ehrenmark 2005).

The procedure used to find the bed shapes leading to the lowest value of $\mathscr{C}$ is now described. In (5.2) the *PQ* weighting coefficients, $\alpha_{p,q}$, are considered free variables in a numerical optimisation procedure whose objective function is the cloaking factor, $\mathscr{C}$. Thus the procedure aims to find the minimum value of $\mathscr{C}$ over all $\alpha_{p,q}$ in *PQ*-dimensional space. For the MSE results, the optimisation has been performed using the NAG routine E04JYF, a quasi-Newton algorithm. For the FLT results, a freely available well-documented piece of software PRAXIS (http://people.sc.fsu.edu/~jburkardt/f77_src/praxis/praxis.html) based on the popular algorithm described by Brent (2002) has been used. Both routines minimise a scalar

function of several variables without needing to calculate derivatives explicitly. Both codes require initial guesses for the vector input and, like all minimisation routines, the minimisation can be sensitive to that initial guess, especially for higher-dimensional parameter spaces.

The principle strategy to be adopted, and applied to the MSE approach initially, involves increasing the number of free variables (hence P and Q) in small increments starting with $P = Q = 1$ where the optimisation is easily performed. At each increment in P and/or Q the optimiser is initialised with the set of coefficients $\alpha_{p,q}$ derived from the previous optimisation, with additional coefficients set to zero. This strategy clearly implies that $\mathscr{C}$ is set on a decreasing path. If one were to assume a classical convergence of this scheme, one might expect the increments in the degrees of freedom at each step of the optimisation to have a smaller and smaller effect on coefficients determined by the previous step and that, in this way, it is easy for the optimiser to find the new minimum at each stage of the process. However, we find that this is not always the case. As the number of free variables, and hence the size of parameter space, is increased multiple local minima emerge and the global minimum can reside in a completely new part of parameter space. The manner in which this happens is not easy to identify or analyse and thus we find ourselves supplementing the procedure described above with a combination of other somewhat *ad hoc* approaches aimed at locating global minima and hence the solution with the lowest $\mathscr{C}$. These are referred to at various points in the description which follows.

5.2. *Axisymmetric beds*

In the original numerical experiments of Porter (2011) and Newman (2012) the possibility of using axisymmetric beds was overlooked because they were not considered likely candidates for cloaking. Whilst the best cloaking results will be shown to be associated with non-axisymmetric beds, it is a more natural starting point to consider axisymmetric beds first. With axisymmetry, $Q = 1$ and the results are independent of the incident-wave angle β. We fix $k_0 h_0 = 1$ and $a/h_0 = 1/2$, $b/h_0 = 5$ and increase P in steps. When $P = 1$ and $\alpha_{1,1}$ is the only free weighting coefficient figure 1(*a*) shows that $\mathscr{C} < 1$ for $k_0 h_0 = 1$ with $\alpha_{1,1} = 0.1$ and that there is close agreement between the MSE and FLT results. We find that $\alpha_{1,1} \approx 0.11$ minimises $\mathscr{C}$ to a value of approximately 0.83. The results of the optimisation procedure for $Q = 1$ and increasing $P = 2, 4, 8$ are summarised in the first three rows of table 1. This table includes two calculations of $\mathscr{C}$ performed under FLT corresponding to the two definitions in the right-hand side and middle parts of (2.9). The difference between these two results, shown in the final column of table 1, act as an indicator of the accuracy of the results using the single-precision WAMIT solver, a point we return to shortly. For FLT, we use the maximum computed value of the two versions of $\mathscr{E}$ defined in (2.9) as the objective function to be minimised and subsequently report just the maximum of the two versions of $\mathscr{C}_{FLT}$. From table 1 both the MSE and FLT cloaking factors are seen to decrease as P is increased. However the values of $\alpha_{p,1}$ to which the optimiser converges can be quite different, especially for larger P.

At this point we note that the WAMIT solver which is used to implement the boundary-element method for the FLT uses single-precision code. The differences in the values of $\mathscr{C}_{FLT}$ computed by the two different methods shown in table 1 can be used to indicate the level of accuracy of the computations. Given these data, and the fact that $\mathscr{C}$ is defined as a factor normalised by $\mathscr{E}_{cyl} = 0.090\,372$, it is difficult to justify reporting values of $\mathscr{C}$ below approximately 0.000 01.

Q	P	$\mathscr{C}_{MSE}$	$\mathscr{C}_{FLT}(1)$	$\mathscr{C}_{FLT}(2)$	(1)–(2)
1	2	0.528 46	0.422 80	0.423 15	−0.000 35
1	4	0.050 79	0.023 43	0.023 61	−0.000 18
1	8	0.000 86	0.000 06	0.000 64	−0.000 58
2	2	0.180 27	0.112 07	0.112 31	−0.000 24
2	4	0.046 48	0.015 23	0.015 34	−0.000 11
2	8	6×10^{-6}	0.000 08	0.000 05	0.000 03
4	2	0.092 56	0.064 25	0.064 49	−0.000 24
4	4	1×10^{-5}	0.003 69	0.003 79	−0.000 10
4	8	1×11^{-11}	0.000 01	0.000 03	−0.000 02

TABLE 1. Cloaking factors optimised under MSE and FLT with varying numbers of radial (P) and azimuthal (Q) basis modes. Here $a/h_0 = 1/2$, $k_0 h_0 = 1$, $b/h_0 = 5$. The first three rows ($Q = 1$) are axisymmetric beds. Columns labelled (1) and (2) indicate $\mathscr{C}_{FLT}$ computed using the first and second alternative relations of (2.9) respectively; the final column shows the difference between them.

We need also to note our experiences of using the MSE numerical method. Despite being written using a double-precision code, like WAMIT it too uses a grid-based discretisation upon which results are dependent. As previously stated, (2.9) is satisfied automatically in the MSE method and cannot be used to gauge the accuracy of the results. In numerical experiments it was found that increasing the refinement of the grid could affect the expansion coefficients found under optimisation quite significantly but that optimised values of $\mathscr{C}$ were much more robust to changes in discretisation. For example, if $\mathscr{C}$ was found to be $O(10^{-11})$ for one discretisation, doubling the grid refinement would still result in a value for $\mathscr{C}$ of $O(10^{-11})$ even though the value of the expansion coefficients for the bed might have changed by as much as $O(10^{-3})$. Given our experiences we feel comfortable reporting the levels of accuracy for $\mathscr{C}_{MSE}$ in table 1.

In figure 2(*a–c*) we show the radial depth profiles for cloaking-optimised axisymmetric beds under MSE and FLT for $Q = 1$, $P = 2, 4, 8$ modes, corresponding to the data in table 1. The bed profiles show reasonably good agreement for 2 and 4 radial modes. When $P = 8$ is used, the FLT finds a local minimum $\mathscr{C} = 0.0065$ when the optimiser is initialised with the MSE coefficients, which is a fairly close fit to the MSE-optimised bed. However, the FLT optimiser finds a lower value of $\mathscr{C} = 0.0006$ when initialised with $P = 4$ FLT-optimised coefficients. It is believed that this represents the global minimum. In the MSE optimisation, the same minimum value is found irrespective of the initialisation of the coefficients.

Despite the superficial similarity in shape of the optimised MSE and FLT bed profiles shown in figure 2(*a–c*) the values of $\mathscr{C}$ computed from one approach using coefficients optimised under the other approach are not always so close. For example, with $Q = 1$, $P = 4$, the value of $\mathscr{C}$ computed using FLT with the coefficients optimised under MSE is 0.194, an order of magnitude higher than the optimised value of $\mathscr{C}_{FLT}$ shown. This illustrates the sensitivity of $\mathscr{C}$ to the bed shape and partly explains why the optimised cloaking factors and bed shapes predicted by the MSE method can appear such a long way from those computed under FLT, especially for more complicated bed shapes.

Figure 2(*a–c*) indicates that the introduction of new degrees of freedom in the optimisation procedure allows the optimiser to locate completely different looking
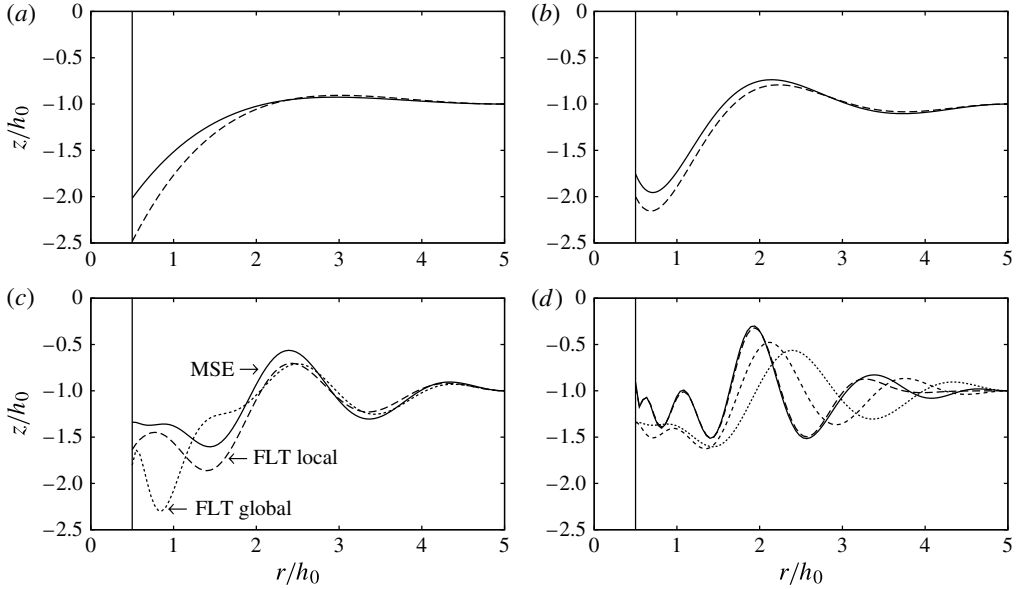
FIGURE 2. Radial depth profile of axisymmetric beds optimised under MSE (solid line) and FLT (dashed) for $Q = 1$ and (*a*) $P = 2$, (*b*) $P = 4$, (*c*) $P = 8$; $a/h_0 = 1/2$, $b/h_0 = 5$, $k_0 h_0 = 1$. The coefficients and values of $\mathscr{C}$ are shown in table 1. In (*c*) local and global minima under FLT are shown. In (*d*) we show just MSE-optimised beds for $P = 8$ (dotted) $P = 10$ (short dashed) $P = 12$ (long dashed) $P = 16$ (solid).

bed shapes. In figure 2(*d*) beds optimised under the MSE method are shown for $P = 8, 10, 12$ and 16 modes. The value of $\mathscr{C}$ drops to under 10^{-7} for $P = 12$ and less than 10^{-11} for $P = 16$. These optimised beds for larger values of P perform poorly under FLT, the increasing oscillations in the bed leading to higher bed gradients where the MSE approximation becomes less accurate. However, figure 2(*d*) does suggest that bed shapes do eventually converge with increasing P although it is not clear if these beds are optimised to a local minimum. Increasing P under FLT to a value of $P = 16$ reduces only slightly the optimised value of $\mathscr{C}_{FLT}$ from its $P = 8$ value. There are a number of reasons why this might happen. It could be that $\mathscr{C}_{FLT}$ reaches a non-zero limit as P increases and perfect cloaking by axisymmetric beds is not possible. Or it could be that the optimiser for $P = 16$ has not found a global minimum. Or it might be that the computation of $\mathscr{C}_{FLT}$ is obscured by numerical inaccuracies.

Figure 3 shows curves of $\mathscr{C}$, for the beds optimized at $k_0 h_0 = 1$, for a range of values of $k_0 h_0$. Results are shown for the $P = 2, 4, 8$ axisymmetric beds as displayed in figure 2. Despite having found that values of $\mathscr{C}$ are very sensitive to the bed shape, once a near-cloaking bed shape has been fixed by a minimisation of $\mathscr{C}$ for a particular wavenumber ($k_0 h_0 = 1$ in these cases) the curves in figure 3 illustrate that the cloaking factor is reduced well below unity across a significant range of wavenumbers.

We next consider the effect of the size of the annular cloaking domain. Now $Q = 1$, $P = 8$, $a/h_0 = 1/2$ are fixed and the axisymmetric beds are optimised for cloaking at $k_0 h_0 = 1$ as before. Figures 4(*a*) and 4(*b*) show the beds optimised under MSE and FLT respectively (note the vertical scales are different) for different values of b/h_0. The curves in these two figures have the same generic bed shape in the outer half of the
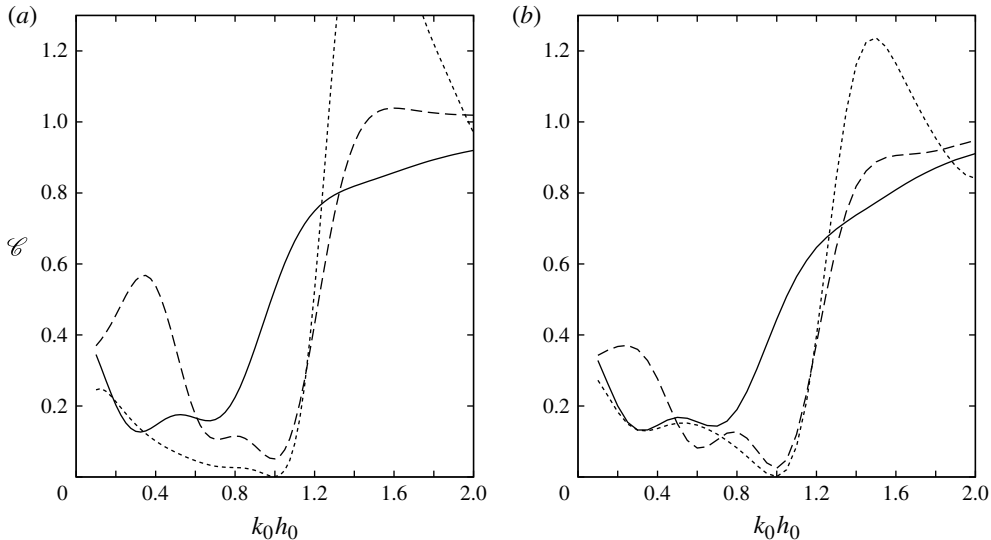
FIGURE 3. Cloaking factor against $k_0 h_0$ for axisymmetric beds optimised by (*a*) MSE and (*b*) FLT with $Q = 1$, $a/h_0 = 1/2$, $b/h_0 = 5$. Curves show varying radial modes: $P = 2$ (solid), $P = 4$ (long dashed) and $P = 8$ (short dashed).

b/h_0	$\mathscr{C}_{MSE}$	$\mathscr{C}_{FLT}$
6	0.005 90	0.020 44
5	0.000 86	0.001 22
4	0.000 02	0.000 28
3	0.000 29	0.000 02
2	0.098 40	0.011 43

TABLE 2. Cloaking factors optimised under MSE and FLT for axisymmetric beds with varying cloaking domain radius, b/h_0. Here $a/h_0 = 1/2$, $k_0 h_0 = 1$, $Q = 1$, $P = 8$.

domain although, as discussed previously, the coefficients optimised under MSE are quantitatively quite different from those optimised under FLT. The detail in the beds close to the cylinder is very different and often associated with larger bed gradients where MSE accuracy breaks down.

The minimised cloaking factors associated with each of the optimised beds in figure 4(*a,b*) for MSE and FLT are shown in table 2. Again, cloaking factors for MSE and FLT do not show much quantitative agreement due to the sensitivity of cloaking to the model and the bed shape. However, they do share the feature that there is a minimum value of $\mathscr{C}$, in this case where the number of radial modes is fixed at $P = 8$, for a value of b/h_0 in the range from 2 to 6. In particular, the cloaking factor using FLT is reduced to a value at the practical limit of the WAMIT solver for $b/h_0 = 3$.

Figure 5 mirrors figure 3 in that it shows the variation of $\mathscr{C}$ with $k_0 h_0$, for beds with $b/h_0 = 2, 3, 4, 5, 6$, optimised under both MSE and FLT. As before it confirms that there is a reduction in $\mathscr{C}$ over a significant range of values of the wavenumber.

In practical applications to offshore structures the mean drift force is an important physical parameter. This is a second-order quantity which measures the time-averaged
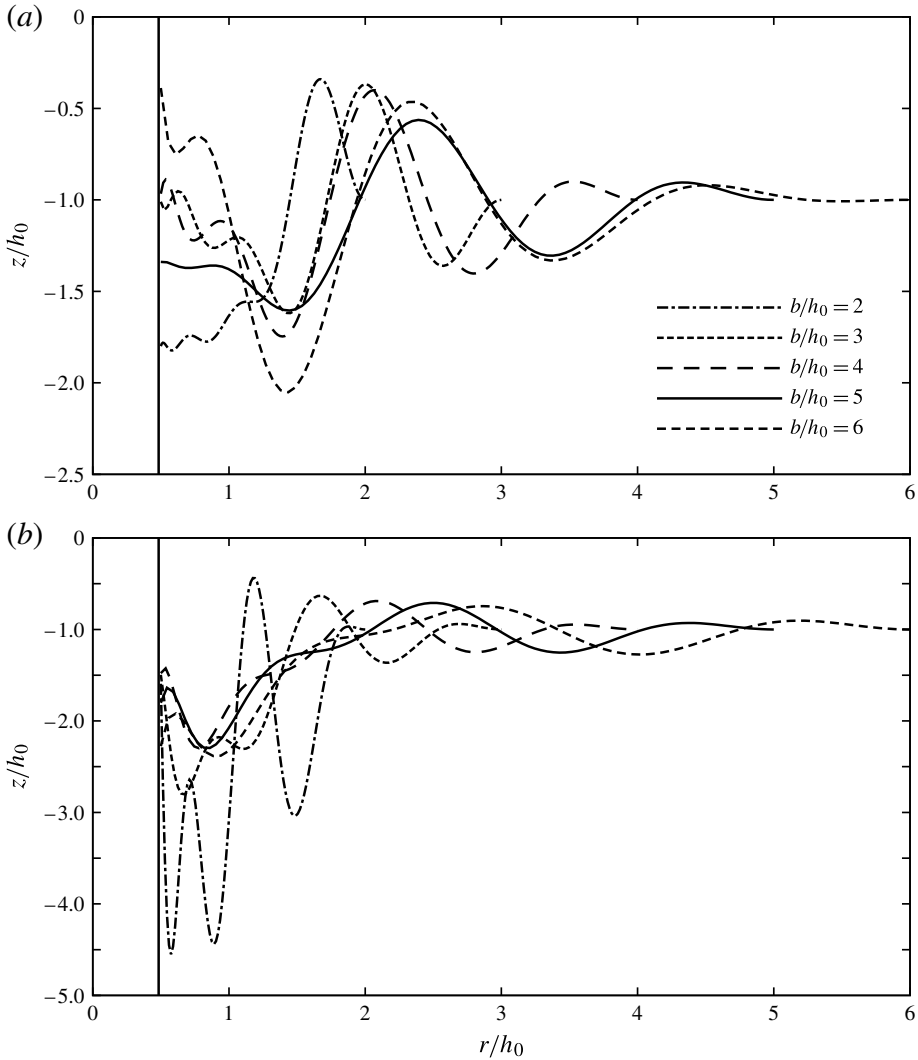
FIGURE 4. Radial depth profiles of axisymmetric beds optimised by (*a*) MSE and (*b*) FLT for $Q = 1$, $P = 8$ with $a/h_0 = 1/2$, $k_0 h_0 = 1$, for five different values of the bed radius b.

pressure force on the scattering surface. Since it can be calculated from the momentum flux in the far field, there is a connection between the mean drift force and the radiated wave amplitude (cf. Mei 1983, § 7.10, (10.21)). Thus perfect cloaking of the cylinder by the undulating bed implies a zero mean drift force on the combined surfaces of the cylinder and the bed. This is illustrated in figure 6(*a*), which shows the drift force on the cylinder and bed, normalized by the corresponding force on the uncloaked cylinder, for the optimized beds with cloaking factors shown in figure 5(*b*). The drift force is practically zero at $k_0 h_0 = 1$, and it is reduced relative to the uncloaked cylinder over a significant range of wavenumbers. As in the case of the scattering energy, the total mean drift force on the cylinder and the bed is positive-definite, but the drift force on the cylinder alone can be negative as shown in figure 6(*b*), with a compensating positive force on the bed.
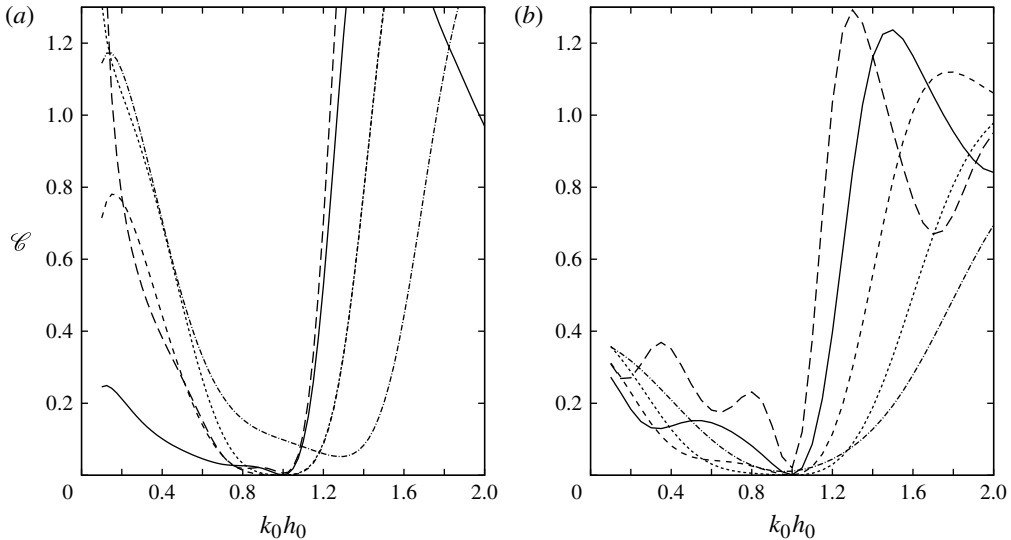
FIGURE 5. Cloaking factor against $k_0 h_0$ for axisymmetric beds optimised by (*a*) MSE and (*b*) FLT with $Q = 1$, $P = 8$, $a/h_0 = 1/2$. Curves show: $b/h_0 = 6$ (long dashed); 5 (solid); 4 (short-dashed); 3 (dotted); 2 (chained).

5.3. *Non-axisymmetric beds*

The results in the previous section show that the cloaking factor can be reduced to values close to zero when the bed is axisymmetric. Whilst the MSE results appear to indicate that $\mathscr{C}$ will continue towards zero as more degrees of freedom are allowed in the bed shape, the FLT results are less clear in this respect. There is certainly no obvious mathematical or physical explanation as to why perfect cloaking should occur with purely axisymmetric bathymetry. Indeed, the low cloaking factors obtained for axisymmetric beds could be regarded as unexpected, hence the reason they were not considered in the earlier studies of Porter (2011) and Newman (2012).

We therefore continue to gather evidence for cloaking by considering non-axisymmetric beds. Our focus continues on the same example of $a/h_0 = 1/2$, $b/h_0 = 5$ and cloaking at $k_0 h_0 = 1$, but now $Q > 1$.

In particular, combinations of values of $P = 2, 4, 8$ and $Q = 2, 4$ have been considered using both the MSE and FLT. The objective for each set of values of (Q, P) considered is to find the lowest valid value of $\mathscr{C}$ using different initial values of the coefficients $\alpha_{p,q}$. These initial values were chosen in many different ways to attempt to find the lowest minimum. One approach uses previously optimised sets of coefficients with smaller values of Q or P (or both). Another uses the MSE-optimised coefficients to initialise an optimisation for the FLT. Occasionally the best results were found by initialising $\alpha_{p,q} = 0$ for all p, q. The results also had to be carefully analysed. In some cases, optimisation of $\mathscr{C}$ corresponds to large values of $\alpha_{p,q}$ which describe beds with large-amplitude oscillations. In other cases, the optimised beds would approach the free surface and the optimisation is stopped.

Results for non-axisymmetric beds are tabulated in the lower section of table 1. Both the MSE and FLT show that the extra degrees of freedom in the bed provided by angular variations lead to a reduction in the cloaking factor. This reduction is generally much more modest with increasing Q than was found with increasing P.
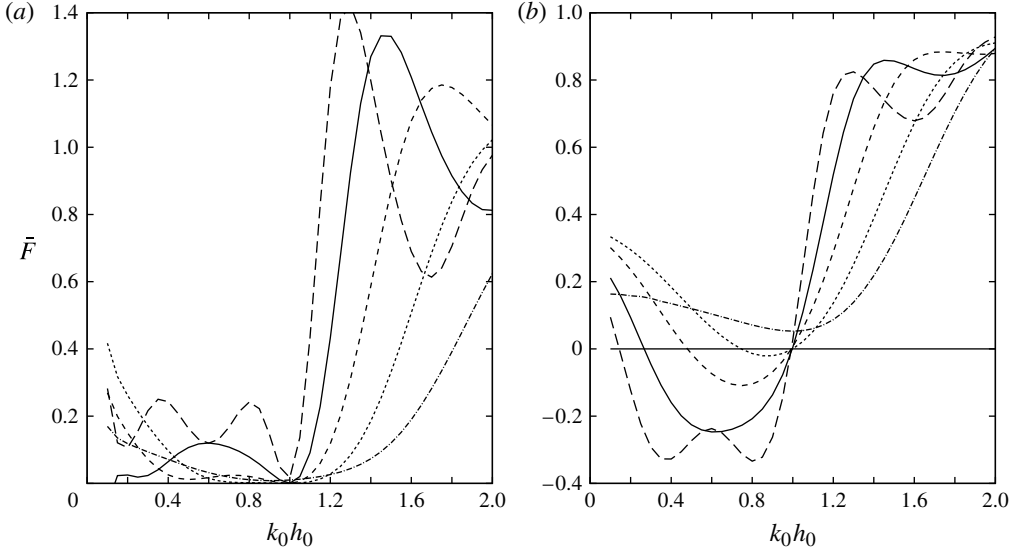
FIGURE 6. Mean drift force $\bar{F}$, normalized by the corresponding force on the uncloaked cylinder for the optimised axisymmetric beds with $Q = 1$, $P = 8$, $a/h_0 = 1/2$. Curves show: $b/h_0 = 6$ (long dashed); 5 (solid); 4 (short-dashed); 3 (dotted); 2 (chained). The total force acting on the cylinder and bed is shown in (a) and the component acting on the cylinder is shown in (b). Values less than one imply a reduced value of the drift force compared to the uncloaked cylinder.

Bearing in mind the reservations set out concerning the accuracy of FLT computations, the results for $(P, Q) = (2, 8)$ and $(4, 8)$ in table 1 do seem to provide a stronger indication of perfect cloaking. As mentioned above, the value of 0.00 001 is at the limits of the estimated accuracy of the FLT code, and it is not possible to say whether the true value may actually be even smaller than this.

Figure 7 shows four bed shapes with the same dimensions, which are optimised using FLT. The number of Fourier/Chebychev coefficients and minimum value of $\mathscr{C}$ are shown for each bed. The cylinder is shown in the centre of each plot, which is cut away to show the profiles of the beds in the $\theta = 0$ and $\theta = \pi/2$ planes. The outer cylindrical boundary is not a physical boundary but the boundary over which the inner and outer regions are matched in the boundary-integral method; it coincides with the outer circle of radius b.

Further numerical experiments carried out, but not reported here, consider cloaking for different values of a/h_0 and $k_0 h_0$. It is found that the optimisation procedure of cloaking described here is robust to changes in these values. As $k_0 a$ is reduced below the value of unity, considered in this paper, cloaking factors reduce towards zero faster with increasing Q, P and vice versa. The undulating bathymetry acts to scatter waves in order to destructively interfere with the waves scattered by the cylinder. For lower values of $k_0 a$ the scattering by the cylinder is dominated by the coefficients of the lower Fourier mode expansion in θ. Thus, it is perhaps not surprising that the undulating bed needs less refinement.

Figure 8 shows the scattered energy $\mathscr{E}$ for the FLT-optimised bed shown in figure 7(d) ($P = 8$, $Q = 4$) for a range of wavenumbers and different angles of incidence between zero and $90°$. (Since the bed possesses planes of symmetry

(*a*) $\mathscr{C} = 0.1123$
(2, 2)

(*b*) $\mathscr{C} = 0.000\,08$
(2, 8)

(*c*) $\mathscr{C} = 0.0153$
(2, 4)

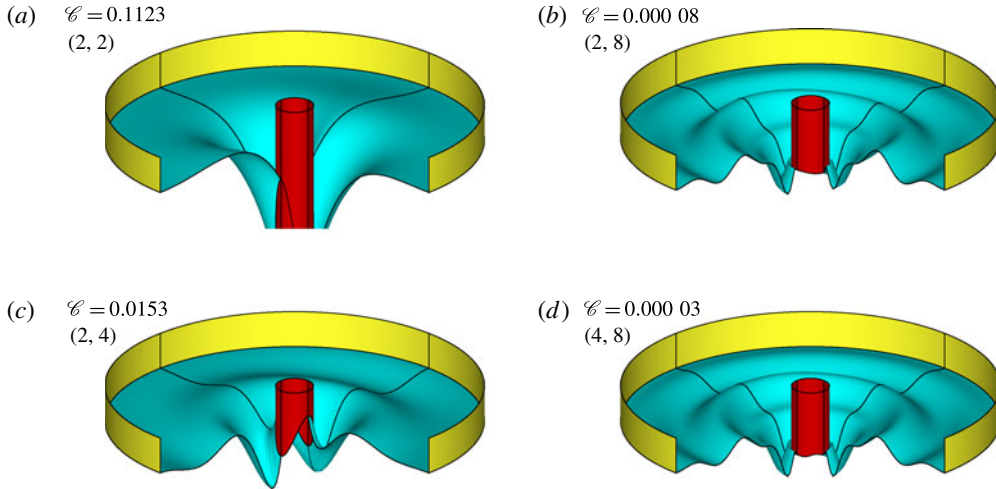(*d*) $\mathscr{C} = 0.000\,03$
(4, 8)

FIGURE 7. (Colour online) Perspective views with cut-aways of non-axisymmetric beds optimised under FLT. The outer cylinder in each figure is the matching boundary S_m as defined in §4. Values of (Q, P) are shown in brackets. Here $a/h_0 = 1/2$, $b/h_0 = 5$, $k_0 h_0 = 1$.

these results extend to all four quadrants of incidence angles.) The scattered energy of the cylinder in a uniform depth is also shown, for comparison. The scattered energy is substantially reduced for wavenumbers less than approximately 1.3, and the dependence on the incidence angle is relatively weak. Similar results have been obtained for the case $P = 8$, $Q = 2$, with somewhat more dependence on the angle of incidence at lower $k_0 h_0$.

6. Conclusions

Numerical evidence has been provided showing that the incident wave energy scattered in diffracted waves by a vertical cylinder over a flat sea bed can be reduced towards zero when the bathymetry in an annular region outside the cylinder is allowed to vary. Results presented here focus initially on axisymmetric beds where this 'cloaking effect' is independent of incident wave direction and where bed profiles are easier to compute, visualise and possibly construct in an experiment. However, much lower cloaking factors have been obtained in computations performed on non-axisymmetric beds suggesting that perfect cloaking requires such bed forms. Two approaches have been described, the first approximate and based on an implementation of the depth-averaged modified mild-slope equations. Numerical optimisation results from this approximation are then used as initial guesses in a method based on full three-dimensional linearised theory. This has required a modification to the boundary-element code WAMIT to account for depressions in the annular cloaking region below the depth of the bed at infinity. In the best example of cloaking under FLT we have produced a reduction in the total scattering cross-section of 10^{-5} over that for a cylinder on a flat bed. This computation is at the practical limit of the program accuracy and it is tempting to conclude that the cloaking factor could be reduced indefinitely towards zero with increasing refinement in the bed shape. This is supported by the results using MSE.

The focus here has been on one particular example of cylinder size $a/h_0 = 1/2$ and wavelength $k_0 h_0 = 1$. With these fixed values, it has been shown that near-cloaking
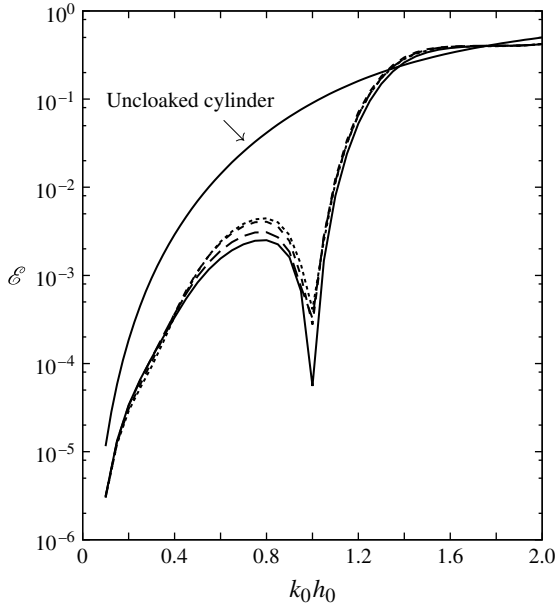
FIGURE 8. Scattered energy $\mathscr{E}$ for the cloaking-optimised non-axisymmetric bed shown in figure 7(*d*) ($a/h_0 = 1/2$, $b/h_0 = 5$, $k_0 h_0 = 1$) for incident wave angles: $\beta = 0$ (solid); $\beta = 30°$ (long dashed); $\beta = 60°$ (short dashed); $\beta = 90°$ (dotted).

occurs for different sizes of the cloaking region b/h_0, in each case with the scattered energy reducing towards zero as the description of the bed shape is increased in refinement. Within these values there is evidence that there are particular values of b/h_0 which minimise the scattering cross-section at a faster rate with increasing modes describing the bed. It could have been possible to include b/h_0 as an additional free parameter in the optimisation procedure to further refine the cloaking process.

It has also been shown that the mean drift force on the cylinder is reduced by cloaking-optimised beds across a significant range of frequencies around the cloaking frequency. This could have some practical significance in the design, for example, of offshore wind turbine foundations.

Further work on cloaking includes replacing the varying bed by other scattering obstacles (Newman 2013). The use of optimisation routines to design marine structures having particular characteristics could be useful in other applications, for example in wave energy capture (e.g. Kurniawan & Moan 2012).

REFERENCES

ALAM, M. 2012 Broadband cloaking in stratified seas. *Phys. Rev. Lett.* **108**, 084502.

ALÙ, A. & ENGHETA, N. 2005 Achieving transparency with plasmonic and metamaterial coatings. *Phys. Rev.* E **72**, 016623.

BELIBASSAKIS, K. A. 2008 A boundary element method for the hydrodynamic analysis of floating bodies in variable bathymetry regions. *Engng Anal. Bound. Elem.* **32**, 796–810.

BRENT, R. 2002 *Algorithms for Minimization with Derivatives*. Dover.

CHAMBERLAIN, P. G. & PORTER, D. 1995 The modified mild-slope equation. *J. Fluid Mech.* **291**, 393–407.

CHAMBERLAIN, P. G. & PORTER, D. 1999 Scattering and near-trapping of water waves by axisymmetric topography. *J. Fluid Mech.* **388**, 335–354.

CHEN, H. & CHAN, C. T. 2007 Acoustic cloaking in three dimensions using acoustic metamaterials. *Appl. Phys. Lett.* **91** (19), 183518.

CUMMER, S. A., POPA, B.-I., SCHURIG, D., SMITH, D. R., PENDRY, J. B., RAHM, M. & STARR, A. 2007 Scattering theory derivation of a 3D acoustic cloaking shell. *Phys. Rev. Lett.* **100**, 024301.

CUMMER, S. A. & SCHURIG, D. 2007 One path to acoustic cloaking. *New J. Phys.* **9**, 45.

EHRENMARK, U. 2005 An alternative dispersion equation for water waves over an inclined bed. *J. Fluid Mech.* **543**, 249–266.

FARHAT, M., ENOCH, S., GUENNEAU, S. & MOVCHAN, A. B. 2008 Broadbanded cylindrical acoustic cloak for linear surface waves in a fluid. *Phys. Rev. Lett.* **101**, 134501.

FARHAT, M., GUENNEAU, S., ENOCH, S. & MOVCHAN, A. B. 2009 Cloaking bending waves propagating in the elastic plates. *Phys. Rev.* B **79** (4), 033102.

FERREIRA, M. D. & NEWMAN, J. N. 2009 Diffraction effects and ship motions on an artificial seabed. In *Proceedings of 24th International Workshop on Water Waves and Floating Bodies, Zelenogorsk, Russia*.

GRIFFITHS, L. S. & PORTER, R. 2012 Focusing of surface waves by variable bathymetry. *Appl. Ocean Res.* **34**, 150–163.

KURNIAWAN, A. & MOAN, T. 2012 Multi-objective optimization of a wave energy absorber geometry. In *Proceedings of 27th International Workshop on Water Waves and Floating Bodies, Copenhagen, Denmark*.

LEE, C.-H. & NEWMAN, J. N. 2004 Computation of wave effects using the panel method. In *Numerical Modeling in Fluid–Structure Interaction* (ed. S. Chakrabarti). WIT Press.

LEONHARDT, U. 2006 Optical conformal mapping. *Science* **312**, 1777–1780.

LIU, H.-W., WANG, Q.-Y. & TANG, G.-T. 2013 Exact solution to the modified mild-slope equation for wave scattering by a cylinder with an idealized scour pit. *ASCE J. Waterway, Port, Coastal, Ocean Engng.* **139**, 413–423.

MARUO, H. 1960 The drift force of a body floating in waves. *J. Ship Res.* **4** (3), 1–10.

MEI, C. C. 1983 *The Applied Dynamics of Ocean Surface Waves*. Wiley Interscience.

MILTON, G. W., BRIANE, M. & WILLIS, J. R. 2006 On cloaking for elasticity and physical equations with a transformation invariant form. *New J. Phys.* **8**, 248.

NEWMAN, J. N. 2012 Scattering by a cylinder with variable bathymetry. In *Proceedings of 27th International Workshop on Water Waves and Floating Bodies, Copenhagen, Denmark*.

NEWMAN, J. N. 2013 Cloaking a circular cylinder in water waves. *Eur. J. Mech.* B (in press); doi: 10.1016/j.euromechflu.2013.11.005.

PENDRY, J. B., SCHURIG, D. & SMITH, D. R. 2006 Controlling electromagnetic fields. *Science* **312**, 1780–1782.

PINKSTER, J. A. 2011 A multi-domain approach in 3-D diffraction calculations *30th International Conference on Ocean, Offshore and Arctic Engineering, Rotterdam, Netherlands*. OMAE2011-49414, pp. 355–364.

PORTER, R. 2011 Cloaking a cylinder in waves. In *Proceedings of 26th International Workshop on Water Waves and Floating Bodies, Athens, Greece*.

PORTER, R. & PORTER, D. 2001 Interaction of water waves with three-dimensional periodic topography. *J. Fluid Mech.* **434**, 301–335.

WARD, A. J. & PENDRY, J. B. 1996 Refraction and geometry in Maxwell's equations. *J. Mod. Opt.* **43** (4), 773–793.

WEHAUSEN, J. V. & LAITONE, E. V. 1960 Surface waves. In *Handbuch der Physik* (ed. S. Flugge), vol. 9, pp. 446–778. Springer.